VIII International Conference on Computational Methods for Coupled Problems in Science and Engineering
COUPLED PROBLEMS 2019
E. Oñate, M. Papadrakakis and B. Schrefler (Eds)

TRIPLY COUPLED ANALYSIS METHOD FOR THIN FLEXIBLE PIEZOELECTRIC BIMORPH IN FLUID

P.C. Ramegowda*, D. Ishihara†, R. Takata†, T. Niho† and T. Horie†

*†Department of Mechanical Information Science and Technology,
680-4 Kawazu, Iizuka, Fukuoka, Japan
e-mail: prakasha@solid.mse.kyutech.ac.jp

Key words: Piezoelectric-structure-fluid interaction, Fluid-structure interaction, Hierarchal decomposition, Partitioned iterative method, Finite element method, Thin piezoelectric bimorph

Abstract. Piezoelectric–structure–fluid interaction is a complex multiphysics coupled phenomena appears wherein piezoelectric devices are in contact or surrounded by the fluid media. The piezoelectric energy harvesting using ocean waves, wind flow, and mechanical vibrations are some of the popular energy savaging methods wherein thin piezoelectric bimorphs surrounded by the fluid is used for power harvesting. With recent advances on micro air vehicles actuated by piezoelectric bimorph actuators in the fluid (surrounding media) as attracted the of piezoelectric–structure–fluid interaction. Generally, in these applications, the piezoelectric bimorph is thin, flexible, and surrounded by the fluid. The large deformation of the thin flexible piezoelectric bimorph causes strong interaction with the electric field (piezoelectric effect) and the surrounding fluid, and inversely, these two fields significantly affect the structure. The piezoelectric field–structure–fluid interaction analysis is very significant. In this work, we propose a hierarchal decomposition method to solve piezoelectric–structure–fluid interaction of a piezoelectric bimorph in the fluid. The proposed method is applied to a flexible restrictor flap in converging channel, where the rubber flap is replaced by the piezoelectric bimorphs made of PVDF or PZT–5H. The resonance frequency of the piezoelectric bimorph in the fluid agrees well with the theoretical and numerical pure FSI cases. These results show a good agreement with the previous studies.

1 INTRODUCTION

The piezoelectric bimorphs are used to actuate the flexible wings of insect–like micro air vehicles. Also, they have attracted great attention in energy harvesting due to their large electro–mechanical convertible characteristics. Generally, in these applications, the piezoelectric bimorph is thin, flexible, and surrounded by the fluid. The large deformation of the thin flexible piezoelectric bimorph causes strong interaction with the electric field (piezoelectric effect) and

the surrounding fluid, and inversely, these two fields significantly affect the structure. The electric field–fluid–structure interaction (EFSI) analysis is very significant.

A novel triply coupled analysis method is proposed to solve the thin flexible piezoelectric bimorph in the fluid. The hierarchal decomposition [1] as the theory is superior to the others in terms of the application to complicated multiphysics problems. Here, the piezoelectric–structure–fluid interaction system is decomposed hierarchically, i.e. it is partitioned into the subsystems of fluid–structure interaction (FSI) and piezoelectric field using the block Gauss–Seidel partitioned iterative method, and then the FSI is split into the fluid–structure velocity field and the pressure filed using an algebraic splitting method [2], and finally, the fluid–structure velocity field is partitioned into the fluid and structure velocity fields using the explicit method for the fluid [3]. Since the structure is quite thin and flexible, MITC4 shell [4] are very well suited for the structural discretization, but modeling electric contribution is a challenging task for shell element. Therefore, the piezoelectric field is solved using 3D solid element, discussed in [5]. The fluid is solved using P1P1 element [6]. The use of these different elements remedies the shortcoming of using the same elements, i.e. the piezoelectric–structure interaction method in Ref. [5] can treat various electric configurations with almost a linear or quadratic distribution of electric potential across the thickness, whereas the shell elements, which are well suited for thin flexible bimorph, cannot treat various electric configurations. The coupled algorithm to solve piezoelectric–structure interaction using finite element methods can be found in Refs. [5, 7–11]. The previous studies of the piezoelectric–structure–fluid interaction can be found in Refs. [12, 13].

The proposed method is applied to a flexible restrictor flap in converging channel [14], where the rubber flap is replaced by the piezoelectric bimorphs made of PVDF or PZT–5H. The resonance frequency of the piezoelectric bimorph actuator analysis in the fluid agrees well with the theoretical and numerical pure FSI cases. However, the frequency shifts upon the connected electric resistive load can be seen for the open–and closed–circuit sensor analysis of the PVDF and PZT–5H bimorph in the fluid. This shift for PVDF is negligible, while this shift for PZT–5H is noticeable. These results show a good agreement with the previous studies [15].

2 GOVERNING EQUATIONS

2.1 Piezoelectricity

The eletromechanical coupling also known as piezoelectric–structure interaction is governed by the constitutive equations written as

$$\sigma_{ij} = C^E_{ijkl} S_{kl} - e_{kij} E_k, \tag{1}$$

$$D_i = e_{ikl} S_{kl} + \varepsilon^S_{ik} E_k, \tag{2}$$

where σ_{ij}, C^E_{ijkl}, S_{kl}, e_{kij}, E_k, and ε^S_{ik} denotes the stress tensor, the elastic constitutive tensor, the mechanical strain tensor, the piezoelectric coupling coefficient, the electric field vector, and the dielectric permittivity tensor, respectively. The relation between the electric field vector E_i

and a scalar electric potential $\phi_{,i}$ is given by

$$E_i = -\phi_{,i}. \tag{3}$$

2.2 Structure

The structure is governed by the Cauchy's equation of motion:

$$\rho^{\mathrm{s}} \frac{\mathrm{d}^2 u_i^{\mathrm{s}}}{\mathrm{d}t^2} = \frac{\partial \sigma_{ji}^{\mathrm{s}}}{\partial x_j} + \rho^{\mathrm{s}} g_i^{\mathrm{s}}, \quad \text{on } {}^t\Omega^{\mathrm{s}}, \tag{4}$$

where ρ^{s}, u_i^{s}, g_i^{s}, and σ_{ij}^{s} denotes the density of the structure, the structural displacement vector, the body force vector acting on the structure, and the 2nd Piola–Kirchhoff stress tensor, respectively. The essential and natural boundary conditions for the stucture is given as

$$v_i^{\mathrm{s}} = \bar{v}_i^{\mathrm{s}}, \quad \text{on } \Gamma_{\mathrm{E}}^{\mathrm{s}}, \tag{5}$$

$$\sigma_{ij}^{\mathrm{s}}.n_j^{\mathrm{s}} = \tau_i^{\mathrm{s}}, \quad \text{on } \Gamma_{\mathrm{N}}^{\mathrm{s}}. \tag{6}$$

where $\Gamma_{\mathrm{E}}^{\mathrm{s}}$ and $\Gamma_{\mathrm{N}}^{\mathrm{s}}$ are complementary subsets of ${}^t\Gamma^{\mathrm{f}}$, $\bar{v}_i^{\mathrm{s}}$ and τ_i^{s} are the prescribed structure velocity and traction values on the complementary subset of ${}^t\Gamma^{\mathrm{s}}$.

2.3 Fluid

The fluid flow is governed by the Navier–Stokes equations for incompressible Newtonian fluids. The arbitrary Lagrangian–Eulerian formulation is employed to describe the incompressible viscous fluid motion in the deformable domain [16]:

$$\rho^{\mathrm{f}} \frac{\partial v_i^{\mathrm{f}}}{\partial t} + \rho^{\mathrm{f}} (v_j^{\mathrm{f}} - \hat{v}_j^{\mathrm{f}}) \frac{\partial v_i^{\mathrm{f}}}{\partial x_j} = \frac{\partial \sigma_{ji}^{\mathrm{f}}}{\partial x_j} + \rho^{\mathrm{f}} g_i^{\mathrm{f}}, \quad \text{in } {}^t\Omega^{\mathrm{f}}. \tag{7}$$

The incompressibility constraint is given as

$$\frac{\partial v_i^{\mathrm{f}}}{\partial x_i} = 0, \quad \text{in } {}^t\Omega^{\mathrm{f}}, \tag{8}$$

where superscript f indicates the fluid components, ρ^{f}, v_i^{f}, $\hat{v}_i^{\mathrm{f}}$, g_i^{f}, and σ_{ij}^{f} denotes the density of the fluid, the fluid velocity vector, the velocity vector of the mesh deformation in ALE co–ordinate, the body force vector acting on the fluid, and the stress tensor of the fluid, respectively.

2.4 Interface conditions

The interaction conditions on the interface between the fluid and the structure are imposed using the following geometric compatibility and equilibrium conditions:

$$v_i^{\mathrm{f}} = v_i^{\mathrm{s}} \equiv v_i^{\mathrm{fs}}, \quad \text{on } \Gamma^{\mathrm{fs}}, \tag{9}$$

$$\sigma_{ij}^{\mathrm{f}}.n_j^{\mathrm{f}} + \sigma_{ij}^{\mathrm{s}}.n_j^{\mathrm{s}} = \tau_i^{\mathrm{f}s}, \quad \text{on } \Gamma^{\mathrm{fs}}, \tag{10}$$

where superscript fs indicates the components of fluid–structure interface, v_i^{fs} and $\tau_i^{\mathrm{f}s}$ denotes the fluid–structure interface velocity vector and the surface force vector acting on the fluid–structure interface, respectively.

3 FINITE ELEMENT FORMULATION OF PIEZOELECTRIC–STRUCTURE–FLUID INTERACTION

The piezoelectric system in 3D solid elements at time $t + \Delta t$ is given by

$$ {}^{t+\Delta t}\mathbf{K}_{\phi\phi}^{(i)} \; {}^{t+\Delta t}\boldsymbol{\phi}_{\text{solid}}^{(i)} = {}^{t+\Delta t}\mathbf{q} - {}^{t+\Delta t}\mathbf{K}_{\phi\text{u}}^{(i)} \; {}^{t+\Delta t}\mathbf{u}_{\text{solid}}^{(i-1)}. \tag{11} $$

where i, $\mathbf{K}_{\phi\phi}$, ϕ_{solid}, $\mathbf{q}$, $\mathbf{K}_{\text{u}\phi}$, and $\mathbf{u}_{\text{solid}}$ denotes block Gauss–Seidel iteration, the matrix of dielectric stiffness matrix of piezoelectric material, the vector of electric potentials in the 3D solid elements, the vector of the external surface density charges on the piezoelectric material, the matrix of the piezoelectric coupling coefficient of the piezoelectric material, and the vector the displacement vector of the 3D solid elements which are evaluated using the displacement transformation method [5]. The displacement are transformed from the shell element to the 3D solid element to analyze the piezoelectric field given as follows [5]:

$$ \mathbf{u}_{\text{solid}} = {}_{\text{u}}\mathbf{T} \; \mathbf{u}^{\text{s}}, \tag{12} $$

where $\mathbf{u}^{\text{s}}$ is the shell element displacement vector and ${}_{\text{u}}\mathbf{T}$ is the displacement transformation matrix. Applying the displacement transformation given in Eq.(12) into Eq.(11) we obtain

$$ {}^{t+\Delta t}\mathbf{K}_{\phi\phi}^{(i)} \; {}^{t+\Delta t}\boldsymbol{\phi}_{\text{solid}}^{(i)} = {}^{t+\Delta t}\mathbf{q} - {}^{t+\Delta t}\mathbf{K}_{\phi\text{u}}^{(i)} \; {}_{\text{u}}\mathbf{T} \; {}^{t+\Delta t}\mathbf{u}^{\text{s}(i-1)}. \tag{13} $$

The induced electrical forces due to the inverse piezoelectric effect can be obtained for the known electric potential in the current BGS iteration i at each time step $t + \Delta t$ in the 3D solid elements as

$$ {}^{t+\Delta t}_{\text{e}}\mathbf{g}_{\text{solid}} = - {}^{t+\Delta t}\mathbf{K}_{\text{u}\phi}^{(i)} \; {}^{t+\Delta t}\boldsymbol{\phi}_{\text{solid}}^{(i)}. \tag{14} $$

The induced electrical forces ${}_{\text{e}}\mathbf{g}_{\text{solid}}$ in the 3D solid of the piezoelectric field are transformed on the shell structure of the FSI system using the force transformation given by

$$ {}_{\text{e}}\mathbf{g}^{\text{s}} = {}_{\text{e}}\mathbf{T} \; {}_{\text{e}}\mathbf{g}_{\text{solid}}, \tag{15} $$

where ${}_{\text{e}}\mathbf{T}$ is the force transformation matrix. Applying the force transformation onto the shell structure of the FSI system, the external force vector acting on the FSI given in Ref. [2] (see Eq.8(f) in [2]) can be rewritten as

$$ \mathbf{g} \equiv \begin{Bmatrix} \mathbf{g}_d^{\text{f}} \\ \mathbf{g}_c^{\text{fs}} \\ \mathbf{g}_d^{\text{s}} \end{Bmatrix} \Longrightarrow \mathbf{g} \equiv \begin{Bmatrix} \mathbf{g}_d^{\text{f}} \\ \mathbf{g}_c^{\text{fs}} + {}_{\text{e}}\mathbf{g}_c^{\text{s}} \\ \mathbf{g}_d^{\text{s}} + {}_{\text{e}}\mathbf{g}_d^{\text{s}} \end{Bmatrix}, \tag{16} $$

where ${}_{\text{e}}\mathbf{g}_c^{\text{s}}$ and ${}_{\text{e}}\mathbf{g}_d^{\text{s}}$ are the external force or transnational force acting on the shell and the external electric moment of force or rotational force acting on the shell, respectively, i.e.,

${}_{\mathrm{e}}\mathbf{g}^{\mathrm{s}} = [{}_{\mathrm{e}}\mathbf{g}^{\mathrm{s}}_{c},\ {}_{\mathrm{e}}\mathbf{g}^{\mathrm{s}}_{d}]^{\mathrm{T}}$. The external transnational force and the rotational forces acting on the shell structure of the FSI system are obtained respectively using

$$ {}_{\mathrm{e}}\mathbf{g}^{\mathrm{s}}_{c} = \sum_{n_r=1}^{N_r} {}_{\mathrm{e}}\mathbf{g}^{n_r}_{\mathrm{solid}} + \sum_{n_s=1}^{N_s} \frac{{}_{\mathrm{e}}\mathbf{g}^{n_s}_{\mathrm{solid}}}{2}, \tag{17} $$

$$ {}_{\mathrm{e}}\mathbf{g}^{\mathrm{s}}_{d} = \sum_{n_r=1}^{N_r} (\mathbf{d}^{n_r} \times {}_{\mathrm{e}}\mathbf{g}^{n_r}_{\mathrm{solid}}) + \sum_{n_s=1}^{N_s} (\mathbf{d}^{n_s} \times \frac{{}_{\mathrm{e}}\mathbf{g}^{n_s}_{\mathrm{solid}}}{2}), \tag{18} $$

where $n_r = 1, \ldots, N_r$, $n_s = 1, \ldots, N_s$, ${}_{\mathrm{e}}\mathbf{g}^{n_r}_{\mathrm{solid}}$, and ${}_{\mathrm{e}}\mathbf{g}^{n_s}_{\mathrm{solid}}$ are the indices of the solid element nodes that are located along the considered director vectors $\mathbf{V}^{k}_{n}$ of the shell nodes, the solid element nodes that are located not along the considered director vector of the shell nodes but directly adjacent to it, the nodal electric force vector at solid node n_r, and the induced nodal electric force vector at solid node n_s. Similarly, $\mathbf{d}^{n_r}$ and $\mathbf{d}^{n_s}$ are the position vectors of the solid element nodes n_r and n_s, respectively, with respect to the shell mid–surface nodes. The details can be found in Ref. [5]. Once the force transformation is done, the FSI is analyzed inside the BGS loop using the projection method proposed by Ishihara and Horie [2]. The time integration of the FSI system is obtained through the predictor–multi–corrector algorithm (PMA) [16, 17]. The stabilization formulation streamline–upwind/Petrov–Galerkin (SUPG) formulations [17] and the pressure–stabilizing/Petrov–Galerkin (PSPG) [6] for incompressible flows are adopted to avoid numerical stability due to the fluid convection and the P1P1 element. Now the increment of intermediate acceleration is determined for the known pressure ${}^{t+\Delta t}\mathbf{p}^{(i)(k-1)}$ using

$$ \mathbf{M}^{*}\Delta\hat{\mathbf{a}}^{(i)} = \Delta\mathbf{g}. \tag{19} $$

Then the intermediate state variables and their increment are evaluated as

$$ {}^{t+\Delta t}\hat{\mathbf{a}}^{(i)(k)} = {}^{t+\Delta t}\mathbf{a}^{(i)(k-1)} + \Delta\hat{\mathbf{a}}^{(i)}, \tag{20a} $$

$$ {}^{t+\Delta t}\hat{\mathbf{v}}^{(i)(k)} = {}^{t+\Delta t}\mathbf{v}^{(i)(k-1)} + \Delta\hat{\mathbf{v}}^{(i)} = {}^{t+\Delta t}\mathbf{v}^{(i)(k-1)} + \gamma\Delta t\Delta\hat{\mathbf{a}}^{(i)}, \tag{20b} $$

$$ {}^{t+\Delta t}\hat{\mathbf{u}}^{(i)(k)} = {}^{t+\Delta t}\mathbf{u}^{(i)(k-1)} + \Delta\hat{\mathbf{u}}^{(i)} = {}^{t+\Delta t}\mathbf{u}^{(i)(k-1)} + \beta\Delta t^{2}\Delta\hat{\mathbf{a}}^{(i)}, \tag{20c} $$

The pressure increment is obtained by solving the pressure Poisson equation (PPE)

$$ \gamma\Delta t\ {}_{\mathrm{T}}\mathbf{G}_{\mathrm{L}}\mathbf{M}^{-1}\mathbf{G}\Delta\mathbf{p}^{(i)} = -{}_{\mathrm{T}}\mathbf{G}^{t+\Delta t}\hat{\mathbf{v}}^{(i)(k)}. \tag{21} $$

The acceleration increment is obtained solving

$$ \gamma\Delta t\ {}_{\mathrm{T}}\mathbf{G}\Delta\mathbf{a}^{(i)} + \mathbf{G}_{\varepsilon}\Delta\mathbf{p}^{(i)} = \Delta\mathbf{h}. \tag{22} $$

The correct phase of the PMA is executed to solve for the acceleration ${}^{t+\Delta t}\mathbf{a}^{(i)(k)}$, the velocity ${}^{t+\Delta t}\mathbf{v}^{(i)(k)}$, and the displacement ${}^{t+\Delta t}\mathbf{u}^{(i)(k)}$ at current BGS and nonlinear iterations of every

time step as follows:

$$^{t+\Delta t}\mathbf{a}^{(i)(k)} = {}^{t+\Delta t}\mathbf{a}^{(i)(k-1)} + \Delta\mathbf{a}, \tag{23a}$$

$$^{t+\Delta t}\mathbf{v}^{(i)(k)} = {}^{t+\Delta t}\mathbf{v}^{(i)(k-1)} + \gamma\Delta t\Delta\mathbf{a}, \tag{23b}$$

$$^{t+\Delta t}\mathbf{u}^{(i)(k)} = {}^{t+\Delta t}\mathbf{v}^{(i)(k-1)} + \beta\Delta t^2\Delta\mathbf{a}, \tag{23c}$$

$$^{t+\Delta t}\mathbf{p}^{(i)(k)} = {}^{t+\Delta t}\mathbf{p}^{(i)(k-1)} + \Delta\mathbf{p}. \tag{23d}$$

At correct stage, we obtain the structural displacements in the shell structure solving Eq.(23c) which can be written as

$$^{t+\Delta t}\mathbf{u}^{\mathrm{s}(i)(k)} = {}^{t+\Delta t}\mathbf{u}^{\mathrm{s}(i)(k-1)} + \Delta\mathbf{u}^{\mathrm{s}(k)}. \tag{24}$$

The resultant displacements in the shell element is now transformed to the solid element using displacement transformation i.e.,

$$^{t+\Delta t}\mathbf{u}^{(i)}_{\mathrm{solid}} = {}_{\mathrm{u}}\mathbf{T}\ {}^{t+\Delta t}\mathbf{u}^{\mathrm{s}(i)}. \tag{25}$$

The components of the transformation matrix ${}_{\mathrm{u}}\mathbf{T}$ are obtained from the displacement interpolation function at time t as in the shell [18] using

$$^{t}\mathbf{u}^{\mathrm{s}}_{j} = h^n(r_1, r_2)\ {}^{t}_{n}\mathbf{u}^{\mathrm{s}}_{j} + \frac{r_3}{2}a\ h^n(r_1, r_2)(-\alpha^n\mathbf{V}^n_2 + \beta^n\mathbf{V}^n_1), \tag{26}$$

where ${}^{t}\mathbf{u}^{\mathrm{s}}_{j}$, ${}^{t}_{n}\mathbf{u}^{\mathrm{s}}_{j}$, n, h^n, and a indicates the displacements of a material point in a shell element at time t with natural coordinates (r_j), the displacement vector of the shell node n at time t, the shell node, the element shape function, and the shell thickness, respectively. α^n and β^n are rotations about $\mathbf{V}^n_1$ and $\mathbf{V}^n_2$, respectively.

4 NUMERICAL EXAMPLE

The proposed method is applied to a flexible restrictor flap in converging channel [14], where the rubber flap is replaced by the piezoelectric bimorphs made of PVDF or PZT–5H, as shown in Fig. 1. The fluid (silicone oil) properties and the fluid boundary conditions are the same with the bench mark problem [2, 14]. The material properties of PVDF and PZT-5H used in the analysis are given in [19, 20]. The theoretical solution for the transverse resonant frequency of the PVDF and PZT–5H bimorph cantilever beam in the vacuum and fluid with the geometric dimensions $L = 0.25\mathrm{m}$, $w = 0.02\mathrm{m}$ and $h = 0.005\mathrm{m}$ evaluated using [21] are as follows:

- PVDF bimorph
  The undamped transverse resonant frequency in the vacuum: $\omega^{(1)}_{\mathrm{vac}} = 85.58\ \mathrm{rad/s}$.
  The damped transverse resonance frequency in the fluid media: $\omega^{(1)}_{\mathrm{fld}} = 52.45\ \mathrm{rad/s}$.
- PZT–5H bimorph
  The undamped transverse resonant frequency in the vacuum: $\omega^{(1)}_{\mathrm{vac}} = 235.64\ \mathrm{rad/s}$.
  The damped transverse resonance frequency in the fluid media: $\omega^{(1)}_{\mathrm{fld}} = 198.69\ \mathrm{rad/s}$.

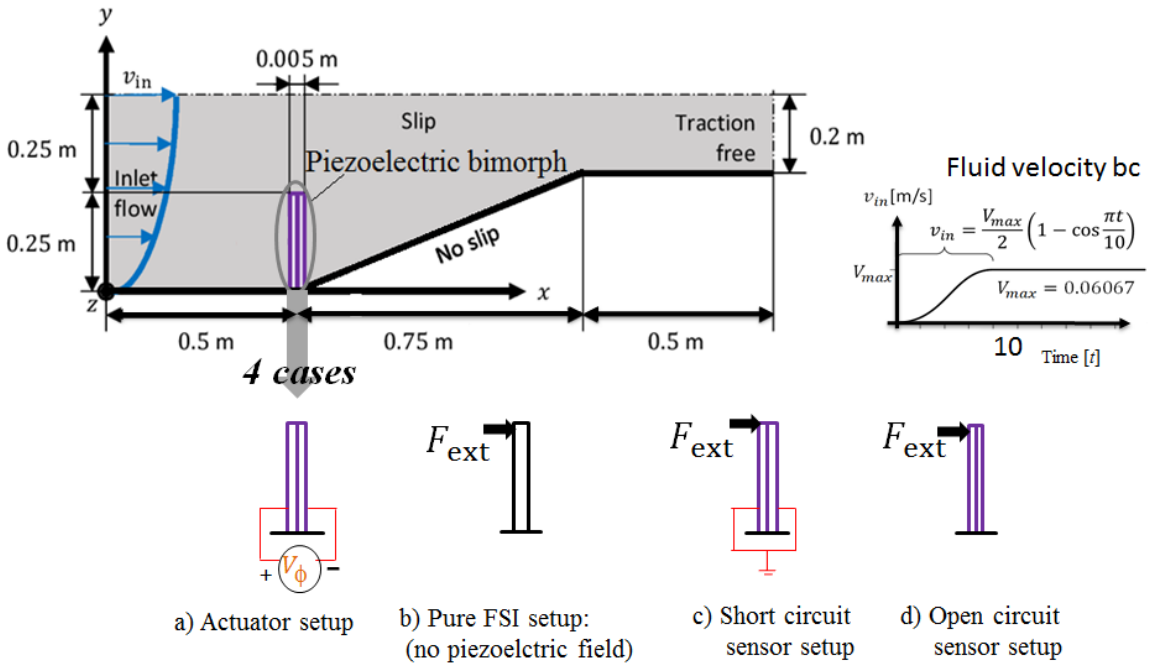

Figure 1: Thin piezoelectric bimorph in converging fluid channel

Fig. 2 shows the frequency response of PVDF and PZT-5H bimorph in converging channel for 4 problem setup in Fig. 1. The simulated results depicted in Fig. 2(a) for PVDF material shows the resonance when the input frequency of the input bias voltage or the frequency of the equivalent external mechanical force F_{ext0} is $\omega_\phi = 50.50$ rad/sec, $\omega = 50.90$ rad/sec, $\omega = 50.10$ rad/sec, and $\omega = 50.30$ rad/sec for case 1, 2, 3, and 4, respectively. The external mechanical force F_{ext0} is evaluated using the blocking force [22] which is equivalent to the electric force generated by the actuator. The vibration amplitudes of the actuator problem setup (case 1) in Fig. 2(a) have less amplitudes compared to that under the pure FSI (case 2), short–circuit sensor configuration (case 3), and the open–circuit sensor configurations (case 4) as the inverse piezoelectric effect counter plays with the mechanical excitation [23]. The resonance obtained with the pure FSI algorithm in case 2 shows a good agreement with the theoretical damped natural frequency i.e. the difference between the theoretical damped natural frequency and the simulated results in case 2 is 2.8%. Now, by taking the FSI solution as an absolute solution, the difference between the FSI (case 2) and piezoelectric-structure-fluid interaction problem (cases 1, case 3, and case 3) is within 1%. This satisfy the approximation condition for the PVDF bimorph given in [23]. This indicates that the frequency shift in the piezoelectric bimorph made of PVDF material upon the electric configuration is negligible. The proposed algorithm takes into account a small shift in the resonance frequency of piezoelectric bimorph made of PVDF which has a negligible shift in the frequency upon the external restive loading, which also appeared in the works of Song et al. [23].

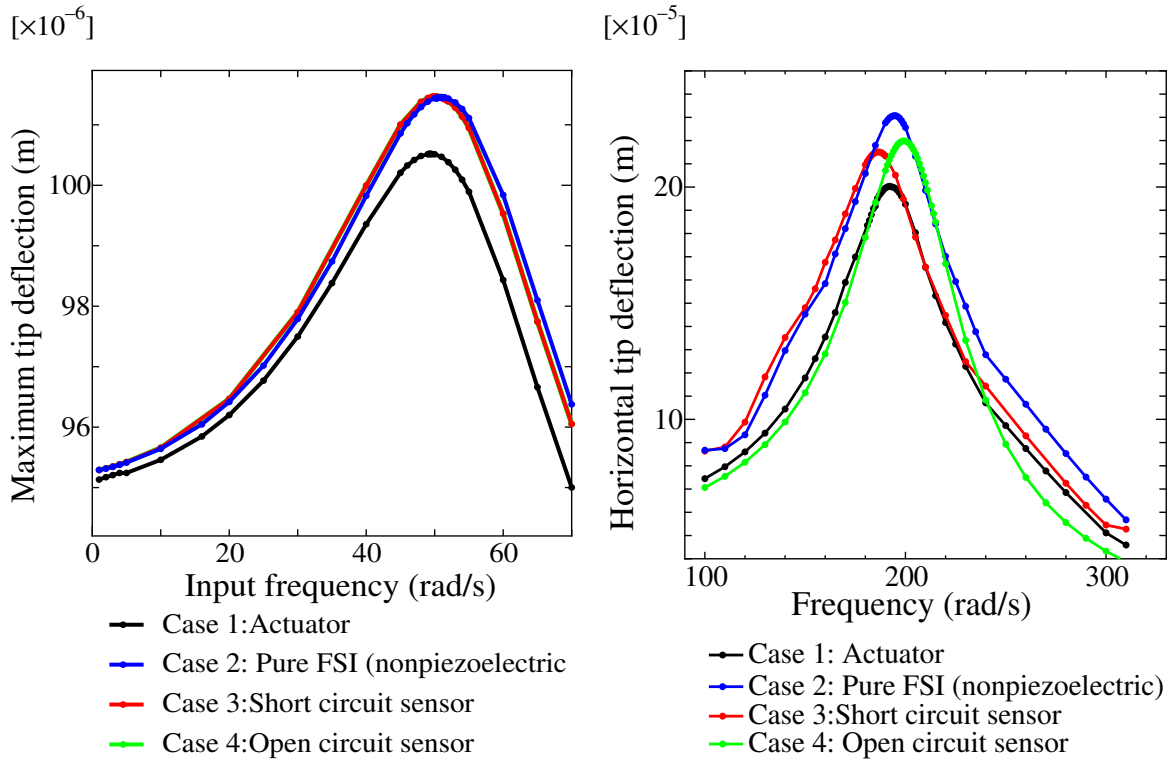

(a) Frequency response of PVDF bimorph

(b) Frequency response of PZT–5H bimorph

Figure 2: Frequency response curve of a piezoelectric bimorph actuator in converging fluid channel at $V_{\phi 0} = 100$V, V_{in} = 0.06067 m/s and $f = 0.05$Hz (v_{in} = $V_{in}(1 - \cos 2\pi ft)$) and pure FSI with external mechanical force at the tip with V_{in} = 0.06067 m/s and $f = 0.05$Hz (v_{in} = $V_{in}(1 - \cos 2\pi ft)$).

The simulated results depicted in Fig. 2(b) for PZT–5H material shows the resonance when the input frequency of the input bias voltage or the frequency of the equivalent external mechanical force $F_{\text{ext}0}$ is $\omega_\phi = 192$ rad/sec, $\omega = 195$ rad/sec, $\omega = 186$ rad/sec, and $\omega = 199$ rad/sec for case 1, 2, 3, and 4, respectively. The difference between open– and closed–circuit resonance frequency is 6.5%, thus justifying the relation given in Ref. [23] for PZT–5H material. The simulation results in [15] also shows 5% difference between the open– and closed–circuit configuration for the piezoelectric bimorph based on PZT–5H material. Therefore, the simulated results using the EFSI algorithm follow the same trends upon the shift in the resonance. Also, the resonance obtained with the FSI algorithm [2] shows a good agreement with the theoretical damped natural frequency. The connected external resistive load decrease the vibration amplitude a bit (by less than 10% [23]) compared to the pure FSI results (case 2) as the inverse piezoelectric effect counter plays the mechanical vibrations. This amplitude dependency upon the external resistive load in PZT–5H piezoelectric bimorph also follows the results presented

by Zhu et al. [15].

5 CONCLUSIONS

A triple coupled algorithm is proposed to analyze the piezoelectric–structure-fluid interaction of a piezoelectric bimorph made of PVDF and PZT–5H material in the viscous fluid media. The proposed method takes into account the triple coupled interaction phenomena. The resonance frequency of a thin flexible piezoelectric bimorph in the fluid agrees well with the theoretical solutions. Also, the shift in the resonance frequency upon the electric boundary conditions is matched well with the theoretical approximations. It is shown that the resonance frequency difference between the open–and closed–circuit sensor mode electric configurations in PVDF piezoelectric bimorphs has a negligible shift. However, a noticeably shift upon the connected external electric resistive load can be seen in PZT–5H piezoelectric bimorphs. The simulated frequency responses and vibration amplitudes of the thin flexible piezoelectric bimorphs analyzed using the proposed EFSI method shows a good agreement with the previous studies.

REFERENCES

[1] D. Ishihara, T. Horie, T. Niho, T. Baba, Hierarchal decomposition for the structure-fluid-electrostatic interaction in a microelectromechanical system., *Computer Modeling in Engineering and Sciences.* **108** (2015) :429–452.

[2] D.Ishihara, T. Horie, A projection method for the monolithic interaction system of an incompressible fluid and a structure using a new algebraic splitting., *Computer Modeling in Engineering and Sciences.* **101** (2014) :421–440.

[3] D.Ishihara, S. Yoshimura, A monolithic approach for interaction of incompressible viscous fluid and an elastic body based on fluid pressure poisson equation., *International Journal for Numerical Methods in Engineering.* **64** (2015) :167–203.

[4] H. Noguchi, T. Hisada, Sensitivity analysis in post buckling problems of shell structures., *Computers & Structures*. **47** (1993) :699–710.

[5] P.C. Ramegowda, D. Ishihara, T. Niho, T. Horie, A novel coupling algorithm for the electric field–structure interaction using a transformation method between solid and shell elements in a thin piezoelectric bimorph plate analysis., *Finite Elements in Analysis and Design. Accepted*, 2019.

[6] T.E. Tezduyar, S. Mittal, S. Ray, R. Shih, Incompressible flow computations with stabilized bilinear and linear equal-order-interpolation velocity-pressure elements., *Computer Methods in Applied Mechanics and Engineering.* **95** (1992) 221–242.

[7] P. C. Ramegowda, D. Ishihara, T. Niho, T. Horie, A novel coupled algorithm for shell structure-electric interaction analysis in mems piezoelectric actuator., *Proceedings of The*

35th JSST Annual Conference International Conference On Simulation Technology. (2016) :332–339.

[8] P.C. Ramegowda, D. Ishihara, T. Niho, T. Horie, Performance evaluation of numerical finite element coupled algorithms for structure–electric interaction analysis of mems piezoelectric actuator., *International Journal of Computational Methods.* **15** (2018) :1850106, 28 pages.

[9] P. Gaudenzi, K.J. Bathe, An iterative finite element procedure for the analysis of piezoelectric continua., *Journal of Intelligent Material Systems and Structures.* **6** (1995) :226–273.

[10] J. Fish, W. Chen, Modeling and simulation of piezocomposites., *Computer Methods in Applied Mechanics and Engineering.* **192** (2003) :3211–3232.

[11] H. Allik, T.J.R. Hughes, Finite element method for piezoelectric vibration., *International Journal for Numerical Methods in Engineering.* **2** (1970) :151–157.

[12] P.C. Ramegowda, D. Ishihara, T. Niho, T. Horie, A finite element approach for a coupled numerical simulation of fluid -structure-electric interaction in mems., *Proceeding of the VII International Conference Computational Methods for Coupled Problems In Science and Engineering.* (2017) :999–1007.

[13] P.C. Ramegowda, D. Ishihara, R. Takata, T. Niho, T. Horie, Fluid–structure and electric interaction analysis of piezoelectric flap in a channel using a strongly coupled fem scheme, *Proceeding of the 6th European Conference on Computational Mechanics (ECCM 6 2018).* (2018) :382–393.

[14] Mok, D. P.; Wall, W. A., Partitioned analysis schemes for the transient interaction of incompressible flows and nonlinear flexible structures., *Trends in Computational Structural Mechanics. CIMNE: Barcelona.* (2001) 689–698.

[15] M. Zhu, E. Worthington, J. Njuguna, Analysis of power output of piezoelectric energy harvesting devices directly connected to a resistive load using a coupled piezoelectric circuit finite element method, *IEEE Transactions on Ultrasonics, Ferroelectrics, and Frequency Control*. **56** (2009) 1309–1317.

[16] T. Nomura, T.J.R. Hughes, An arbitrary lagrangian–eulerian finite element formulation for interaction of fluid and a rigid body., *Computer Methods in Applied Mechanics and Engineering*. **95** (1992) 115–138.

[17] TA. Brooks, T.J.R. Hughes, Streamline upwind/petrovgalerkin formulations for convection dominated flows with particular emphasis on the incompressible navierstokes equation., *Computer Methods in Applied Mechanics and Engineering*. **32** (1982) 199–259.

[18] E.N. Dvorkin, K.J. Bathe, A continuum mechanics based four-node shell element for general nonlinear analysis., *Engineering Computation* **1** (1984) 77–88.

[19] Z. Wang, S. Chen, W. Han, The static shape control for intelligent structures., *Finite Elements in Analysis and Design*. **26** (1982) :303–314.

[20] S. Zhu, B. Jiang, W. Cao , Characterization of piezoelectric materials using ultrasonic and resonant techniques., *Proceeding of SPIE, Medical Imaging:Ultrasonic Transducer Engineering*. **3341** (1998) :154–162.

[21] C.A.Van Eysden, J.E. Sader , Resonance frequencies of a cantilever beam immersed in a fluid, *Journal of Applied Physics*. **100** (2006) :114916,8 pages.

[22] Q.M. Wang, L.E. Cross, Performance analysis of piezoelectric cantilever bending actuator, *Ferroelectrics*. **215** (1998) :187–213.

[23] J. Song, G. Zhao, B. Li, J. Wang, Design optimization of pvdf–based piezoelectric energy harvesters., *Heliyon*. **3** (2017) : e00377, 18 pages.